Supplementary Materials for

A SUMO-ubiquitin relay recruits proteasomes to chromosome axes to regulate meiotic recombination

H. B. D. Prasada Rao, Huanyu Qiao, Shubhang K. Bhatt, Logan R. J. Bailey, Hung D. Tran, Sarah L. Bourne, Wendy Qiu, Anusha Deshpande, Ajay N. Sharma, Connor J. Beebout, Roberto J. Pezza, Neil Hunter*

*Corresponding author. Email: nhunter@ucdavis.edu

Published 5 January 2017 on *Science* First Release
Published 27 January 2017, *Science* **355**, 403 (2017)
DOI: 10.1126/science.aal2690

This PDF file includes

Revision (26 January 2017): In this revision, Fig. S8 been replaced with the correct figure in place of a duplicate Fig. S7. Reference 36 was removed from the First Release, and another reference (*23*) was added. The reference list and relevant text are updated. The originally posted supplementary materials are available here.

Materials and Methods

Mice

All mice were congenic with the C57BL/6J background. Mice were maintained and used for experimentation according to the guidelines of the Institutional Animal Care and Use Committees of the University of California, Davis. The *Hei10 and Rnf212* mutant lines were previously described (*22, 29*).

Cytology

Testes were dissected from freshly killed animals (14 days to 6 months old) and processed for surface spreading of spermatocyte chromosomes as described (*30*). To obtain chromosome spreads from fetal oocytes, ovaries were dissected from 16-18 dpc fetuses and processed as described (*31*). Immunofluorescence staining was performed as described (*32*), using the following primary antibodies with incubation overnight at room temperature: mouse anti-SYCP3 (sc-74568 Santa Cruz, 1:200 dilution), rabbit anti-SYCP3 (sc-33195 Santa Cruz, 1:300), mouse anti-SUMO1 (SUMO-1 21C7, 1:150)(*33*), mouse anti-SUMO2/3 (SUMO-2 8A2, 1:150; SUMO2 and SUMO3 are antigenically indistinguishable)(*34*), rabbit anti-ubiquitin (ab19247 Abcam, 1:200), mouse anti ubiquitin (FK2, Ubiquigent ,1:200), rabbit monoclonal anti-ubiquitin antibody, Lys48-Specific, clone Apu2-07 (Genentech, 1:100), mouse anti-20S proteasome a-subunits (ST1049 Calbiochem,1:150), goat anti-20S proteasome b5 (C-19 Santa Cruz, sc-55009, 1:100), mouse anti-RAD51 (51RAD01 Thermo scientific,1:200), rabbit anti-DMC1 (sc-22768 Santa Cruz, 1:200), rabbit anti-MEI4 (1:200; generously provided by Bernard de Massy, Institut de Génétique Humaine, Montpellier)(*19*), rabbit monoclonal anti-RPA32 (ab76420 Abcam, 1:100), rabbit anti-MER3 (Roberto Pezza, unpublished; 1:500), guinea pig anti-TEX11 (1:100)(*35*), rabbit anti-REC8 (1:300)(*36*), guinea pig anti-RNF212 (1:50)(*22*), rabbit anti-MSH4 (ab58666 Abcam, 1:100), mouse monoclonal anti-CCNB1IP1/HEI10 (ab118999 Abcam, 1:150), mouse monoclonal anti-γH2AX (05-636 Millipore, 1:500). Slides were subsequently incubated with the following goat secondary antibodies for 1 h at 37 °C: anti-rabbit 488 (A11070 Molecular Probes, 1:1000 dilution), anti-rabbit 568 (A11036 Molecular Probes, 1:2000), anti-mouse 555 (A21425 Molecular Probes, 1:1000), anti-mouse 594 (A11020 Molecular Probes, 1:1000), anti-mouse 488 (A11029 Molecular Probes, 1:1000), and anti-guinea pig fluorescein isothiocyanate (106-096-006 FITC, Jackson Labs, 1:200). Coverslips were mounted with ProLong Gold antifade reagent (Molecular Probes). For all quantification, images from two to five animals were captured and analyzed. 12 to 50 nuclei were imaged for each prophase stage, unless stated otherwise. Comparisons were made between datasets obtained from animals that were either littermates, or matched by age. Two observers performed all cytological analyses; the second observer was blind to which group/genotype was being analyzed. SYCP3-staining nuclei were staged using standard criteria (*37*). For quantification of SUMO, ubiquitin and proteasome localization, only foci closely associated with ("touching") the SYCP3-staining chromosome axes were counted; these included foci and flares that emanate from the SYCP3 staining lines, and foci located between synapsed axes. The large staining clusters localized to the sex chromosomes (for SUMO and ubiquitin) and at centromeres (for SUMO only) were not counted as they are mediated by distinct pathways (*Rnf212-Hei10* independent). In some experiments, the

high density of SUMO2/3 and ubiquitin signals precluded focus counting. In these cases, signal intensity signal intensity ratios were calculated for SUMO2/3 and ubiquitin; total axis-associated signal for SUMO or ubiquitin was divided by the signal for SYCP3. Signal intensity ratios for HEI10 foci were calculated by dividing signals for individual HEI10 foci by SYCP3 signals in an adjacent region.

Spermatocyte culture and chemical inhibition

Short-term culture of spermatocytes was performed essentially as described (*14*). Inhibitors were added at the following concentrations: 30 μM 2-D08 (Millipore; 505156; 30 mM stock dissolved in DMSO) (*15*); 10 μM PYR41 (Millipore; 662105; 10 mM stock dissolved in DMSO)(*16*), 10 μM MG132 (Sigma-Aldrich; M8699; 10 mM stock dissolved in DMSO). To induce progression to metaphase I, Okadaic acid (LC Laboratories, 1mM stock in ethanol) was added to a final concentration of 2.5 mM after 20 hrs of culture and cells were incubated for a further 6 hrs (*38*). Cells were then pelleted, washed with PBS and processed for surface spreads. Equivalent volumes of DMSO or ethanol alone were added to "no treatment" control cultures. In all cell culture experiments, cell viability was quantified using the Trypan Blue exclusion assay.

Imaging

Immunolabeled chromosome spreads and DAPI-stained diakinesis/metaphase I nuclei were imaged using a Zeiss AxioPlan II microscope with 63× Plan Apochromat 1.4 NA objective and EXFO X-Cite metal halide light source. Images were captured by a Hamamatsu ORCA-ER CCD camera and processed using Volocity (Perkin Elmer) and Photoshop (Adobe) software packages. SIM analysis was performed using a Nikon N-SIM super-resolution microscope system and NIS-Elements 2 image processing software.

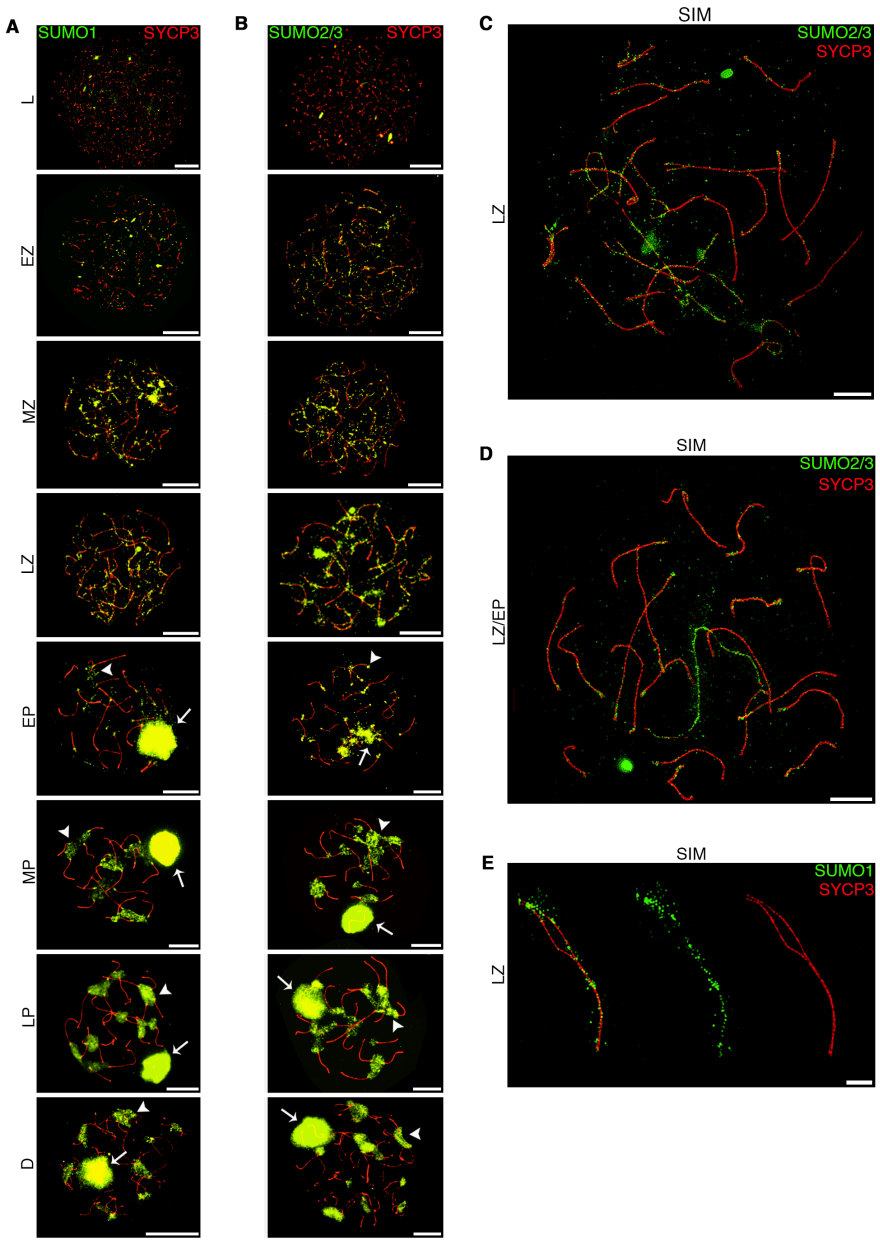

Fig. S1.

SUMO1 and SUMO2/3 immunostaining of prophase mouse spermatocytes. (**A** and **B**) Wild-type spermatocyte nuclei immunostained for SUMO1 or SUMO2/3 (green) and SYCP3 (red). Arrows indicate sex bodies and arrowheads highlight centromeric heterochromatin. (**C** and **D**). Nuclei imaged by SIM. (**E)** Single pair of synapsing chromosomes imaged by SIM. L, leptonema; EZ, early zygonema; MZ, mid zygonema; LZ, late zygonema; EP, early pachynema; MP, mid pachynema; LP, late pachynema; D, diplonema. Scale bars: 10µm in panels A and B, 5µm in C and D, and 1µm in E.

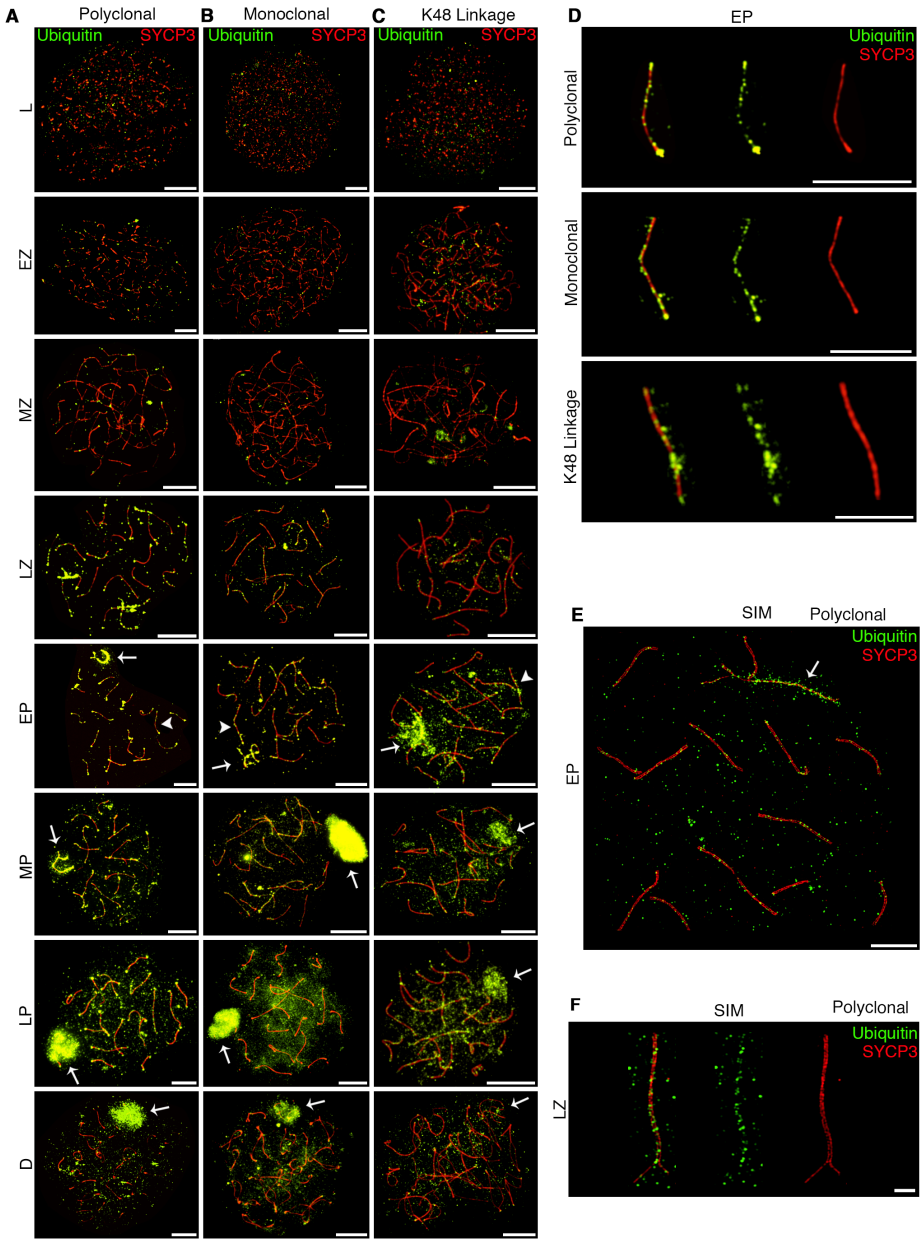

Fig. S2

Ubiquitin immunostaining of prophase mouse spermatocytes. (**A–C**) Wild-type spermatocyte nuclei immunostained with SYCP3 (red) and polyclonal, monoclonal or K48-linkage-specific antibodies against ubiquitin (green). Arrows highlight sex bodies. Arrowheads indicate individual chromosomes magnified in D. (**E**) Early pachynema nucleus imaged by SIM using the polyclonal anti-ubiquitin antibody. Arrows highlight X-Y chromosome pair. (**F**) Single pair of chromosomes with nearly full synapsis imaged by SIM. Scale bars: 10µm in panels A-C, 5µm in E, and 1µm in D and F. L, leptonema; EZ, early zygonema; MZ, mid zygonema; LZ, late zygonema; EP, early pachynema; MP, mid pachynema; LP, late pachynema; D, diplonema.

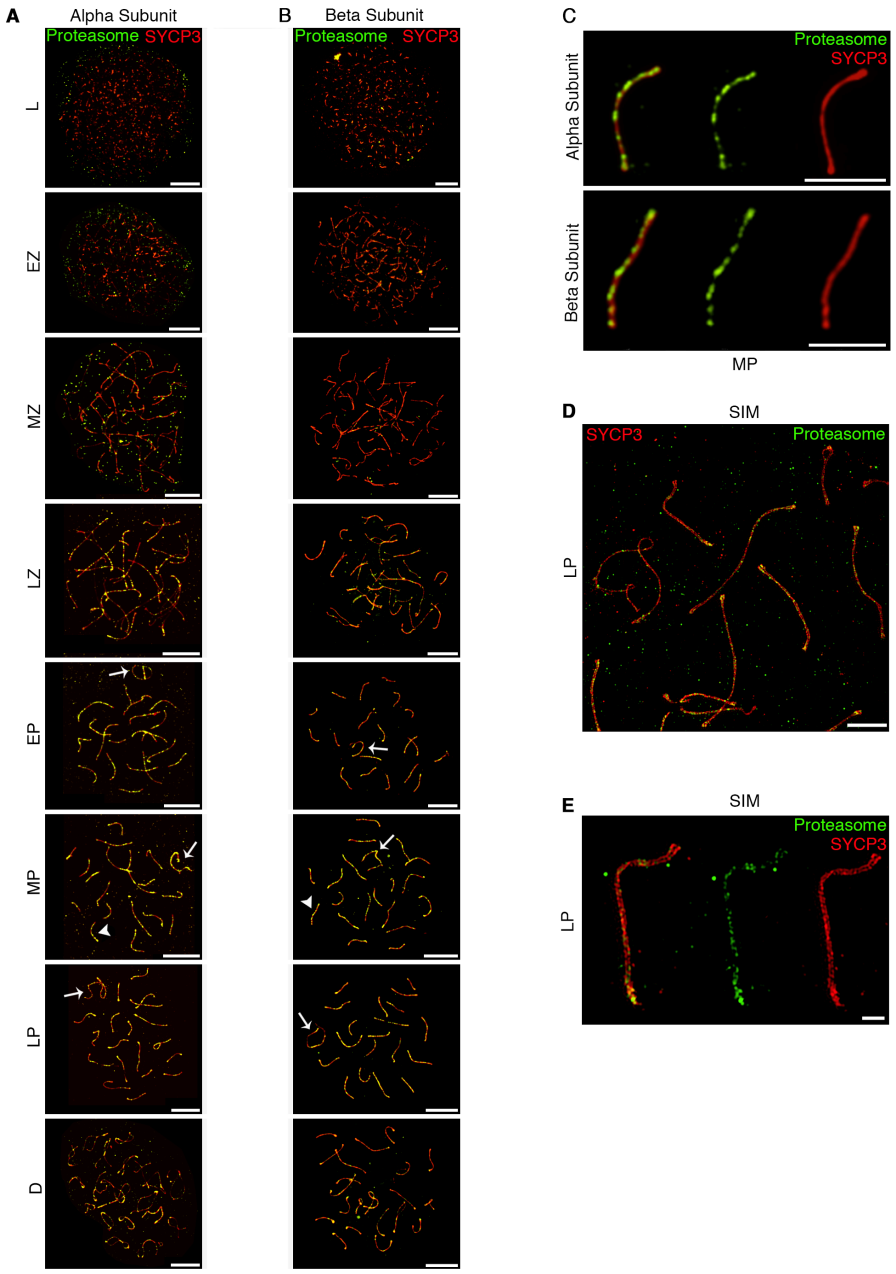

Fig. S3

Proteasome immunostaining of prophase mouse spermatocytes. (**A** and **B**) Wild-type spermatocyte nuclei immunostained with antibodies against the alpha or beta subunits of the 20S particle (green) and SYCP3 (red). Arrows highlight sex bodies. Arrowheads indicate individual chromosomes magnified in C. (**D**) Late pachynema nucleus imaged by SIM using the anti-alpha subunit 20S antibody. (**E**) Single pair of chromosomes from a late pachytene nucleus imaged by SIM. Scale bars: 10μm in panels A and B, 5μm in D, and 1μm in C and E. L, leptonema; EZ, early zygonema; MZ, mid zygonema; LZ, late zygonema; EP, early pachynema; MP, mid pachynema; LP, late pachynema; D, diplonema.

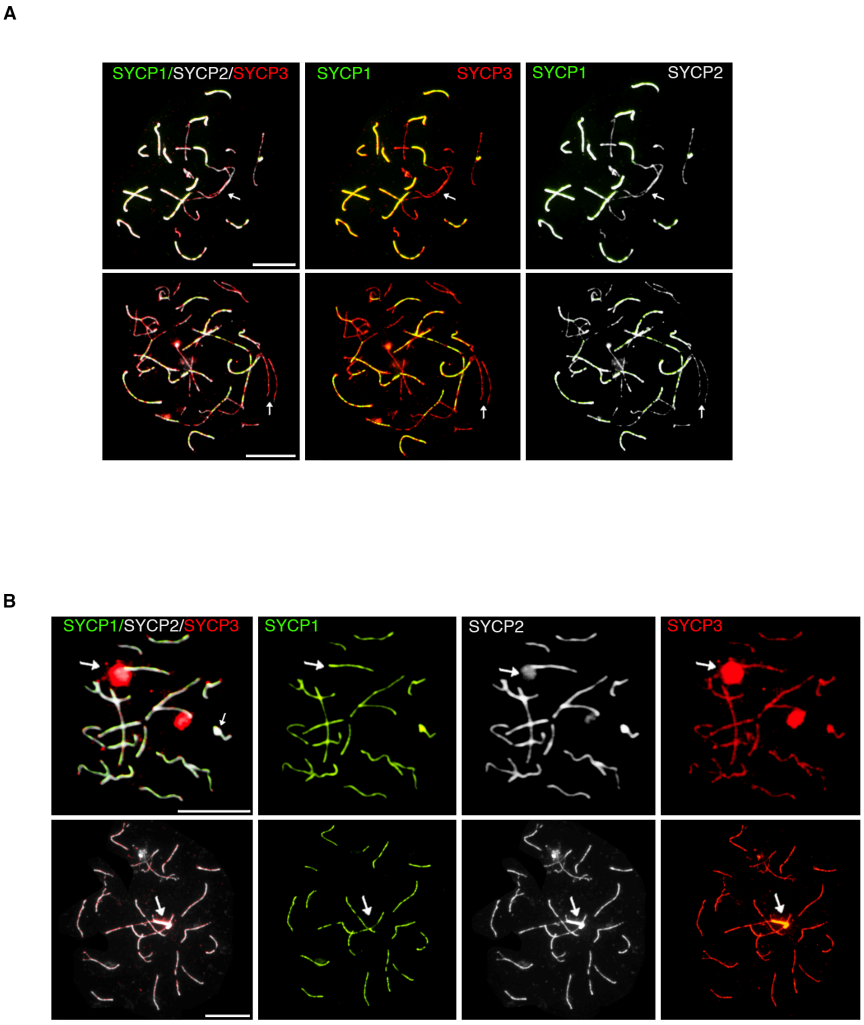

Fig. S4

Characterization of synapsis defects following proteasome inhibition. Examples of spermatocyte nuclei containing synapsis defects (**A**) or SYCP3 aggregates (**B**) following proteasome inhibition with MG132. Nuclei were immunostained for the chromosome axis markers SYCP2 and SYCP3, and the central region component SYCP1. This analysis confirmed that unsynapsed chromosome axes lack SC central region: in 75 nuclei with synapsis defect, none of the unsynapsed axes showed staining for SYCP1. SYCP3 aggregates were found to always include a second axis component, SYCP2, but coaggregation of SYCP1 was much rarer and generally only seen in the smaller aggregates: only 4% of SYCP2/3 (3/75) aggregates contained SYCP1 and these were confined to smaller structures (3/12 aggregates of < 1.3 μm^2). Analogous defects were also seen following inhibition of SUMO and ubiquitin conjugation (not shown). Scale bars: 10µm.

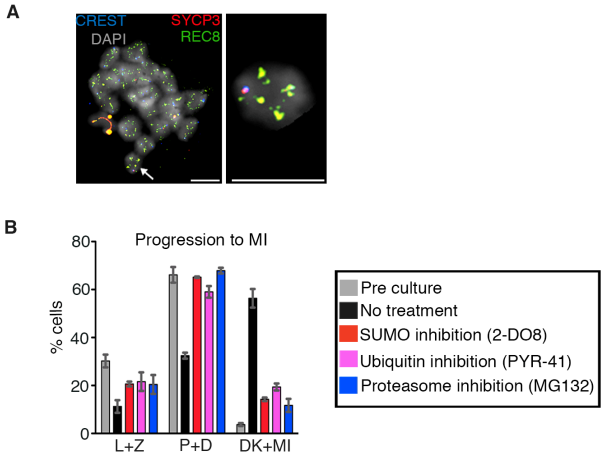

Fig. S5

Inhibition of the SMS or UPS blocks precocious progression into metaphase I. Prophase spermatocytes do not progress beyond diplonema under standard culture conditions, but treatment with the phosphatase inhibitor okadaic acid triggers precocious progression into metaphase I (*38*). We asked whether the block to pachytene exit following inhibition of the SMS and UPS (Fig. 2D) could be overridden by okadaic acid treatment. (**A**) Immunostaining regimen used to distinguish diakinesis and metaphase I nuclei. Surface-spread spermatocyte nuclei were DAPI (grey) and stained immunostained for SYCP3 (red), which is lost from axes during diakinesis and retained only at centromeres in metaphase I; REC8 (green), which marks the cohesion axis and is retained along chromosome arms until anaphase; and CREST (white), which marks kinetochores. (**B**) Quantification of prophase progression following culture with or without inhibitors, and stimulation with Okadaic acid. In the absence of inhibitors, 56% of prophase spermatocytes had progressed to diakinesis/metaphase-I, 6 hrs after addition of okadaic acid, while progression was largely blocked when cells were treated with 2-DO8, PYR41 or MG132. L, leptonema; Z, zygonema; P, pachynema; D, diplonema; DK, diakinesis; MI, metaphase I. Error bars show mean ± s.e.m. Scale bars: 10 μm.

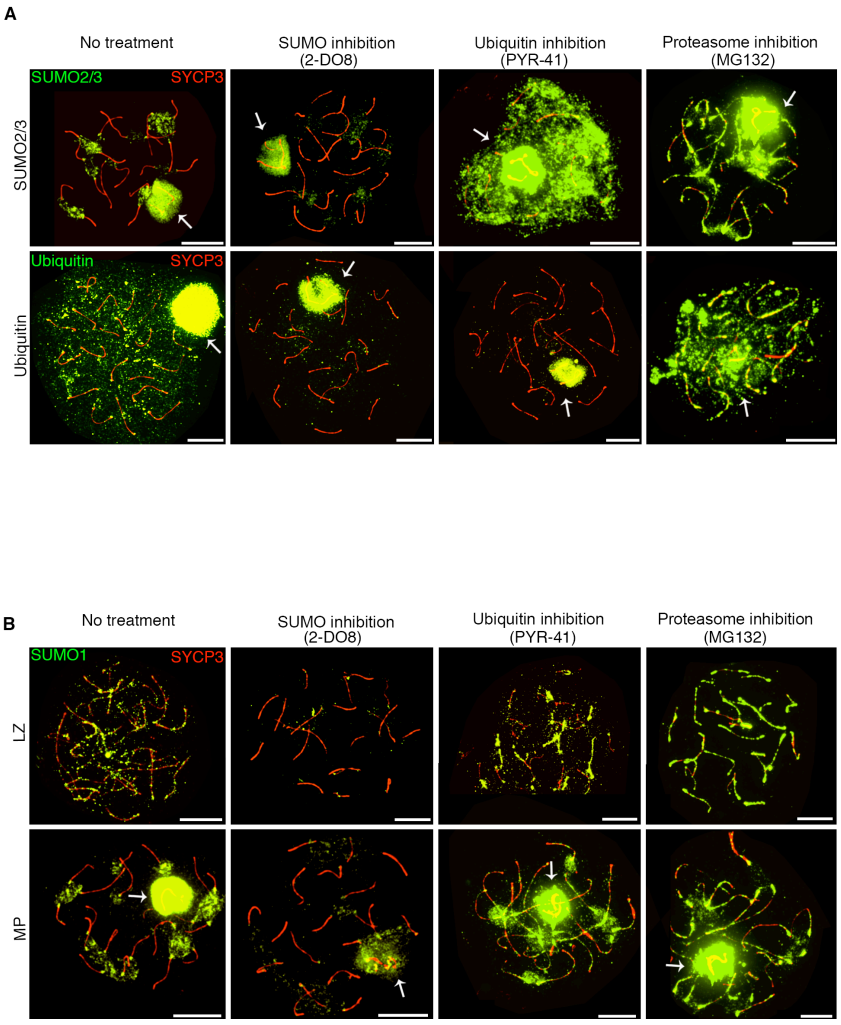

Fig. S6

SUMO and ubiquitin immunostaining in cultured spermatocytes following inhibitor treatments. (**A**) Analysis of mid pachytene spermatocyte nuclei following chemical inhibition of SUMO conjugation, ubiquitin conjugation or proteasomes. Spread nuclei were immunostained for SUMO2/3 or ubiquitin (green), and SYCP3 (red). Abnormal accumulation and persistence of SUMO is seen following inhibition of the UPS (ubiquitylation and proteasomes), with coexistence of axial/chromatin and sex body staining. By contrast, axial staining for ubiquitin is diminished following SUMO inhibition by 2-DO8. We note that weak staining of the sex bodies for SUMO and ubiquitin is still observed following treatment with 2-DO8 and PYR-41, respectively. This may represent conjugation implemented prior to inhibitor treatment and/or incomplete inhibition of SUMO/ubiquitin conjugation. (**B**) Images of spermatocyte nuclei following chemical inhibition of SUMO conjugation, ubiquitin conjugation or proteasomal degradation. Nuclei were immunostained for SUMO1 and SYCP3 (red). Patterns mirror those seen for SUMO2/3: SUMO1 staining is diminished by 2-DO8 and persists following treatment with PYR-41 or MG132. LZ, late zygonema; MP, mid pachynema. Arrows indicate sex bodies. Scale bars = 10μm.

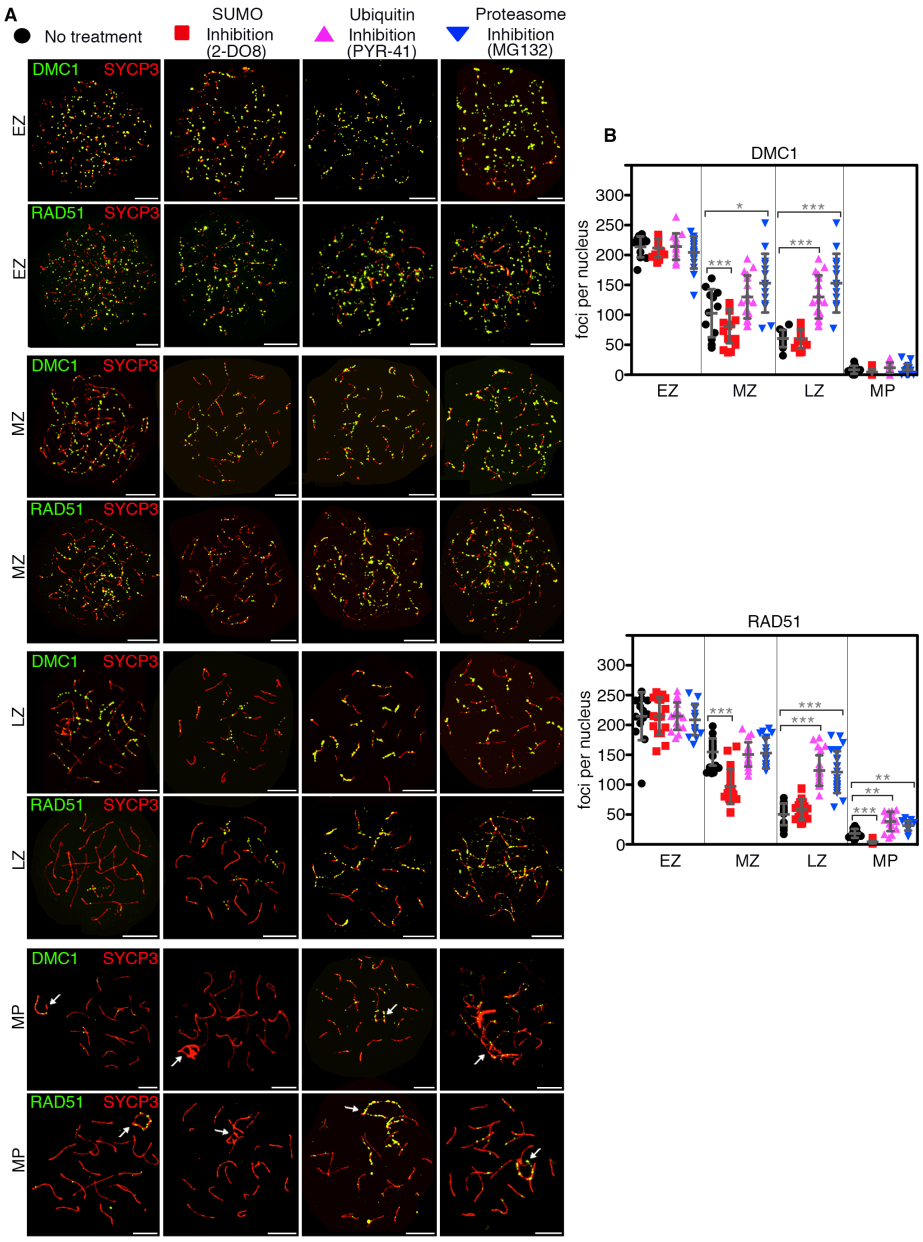

Fig. S7

The SCS and UPS regulate turnover of DMC1 and RAD51. (**A**) Representative images of spermatocyte nuclei immunostained for SYCP3 (red) and either DMC1 or RAD51 (green) following chemical inhibition of SUMO conjugation, ubiquitin conjugation or proteasomes. (**B**) Quantification of DMC1 and RAD51 foci from the experiments represented in panels A , respectively. EZ, early zygonema; MZ, mid zygonema; LZ, late zygonema; MP, mid pachynema. Arrows indicates sex chromosomes. Error bars show mean ± s.d. (*) $P \leq 0.05$, (**) $P \leq 0.01$, (***) $P \leq 0.001$, two-tailed Mann-Whitney test. Scale bars = 10µm.

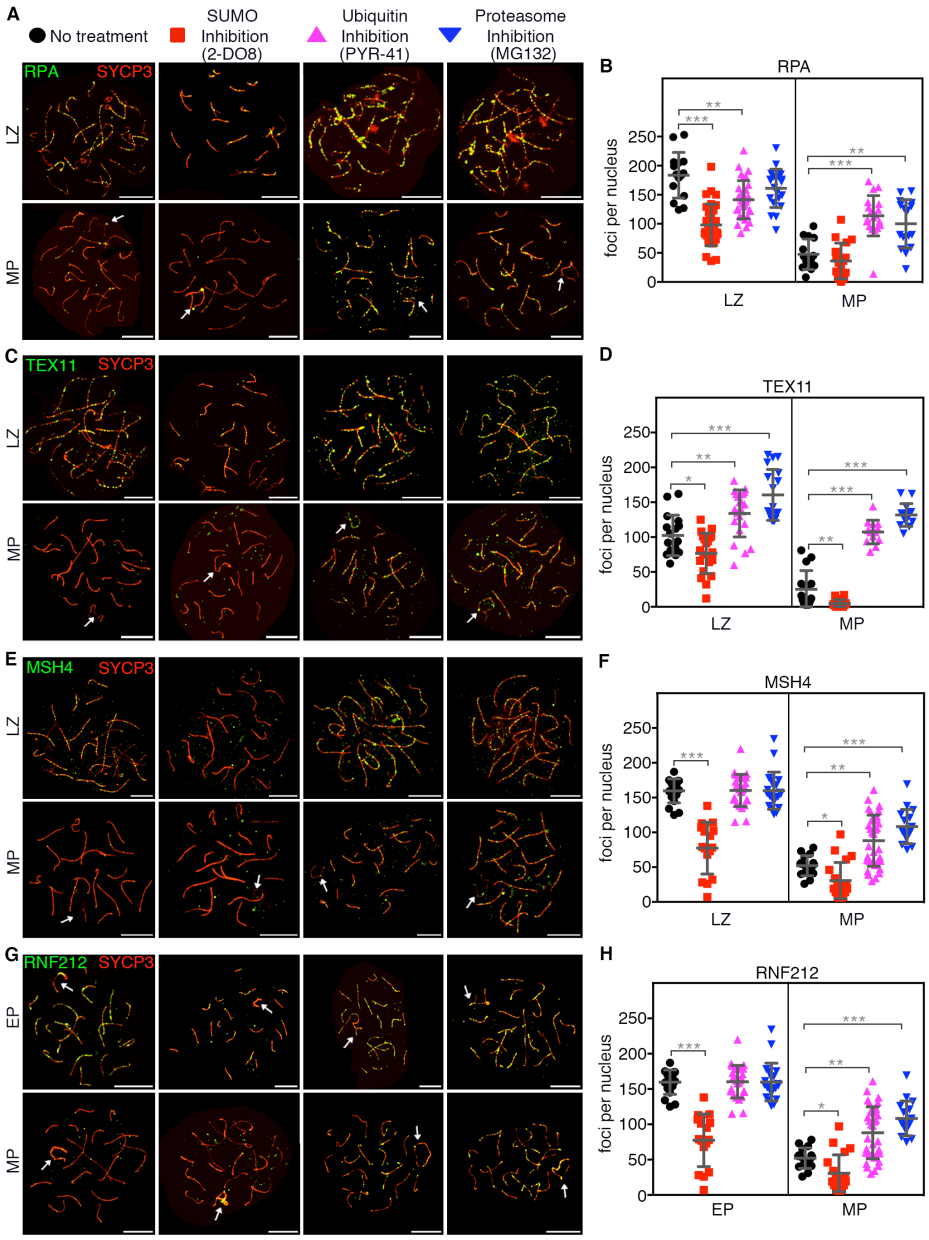

Fig. S8

The SCS and UPS regulate turnover of RPA and the ZMM proteins. (**A, C, E** and **G**) Representative images of spermatocyte nuclei immunostained for SYCP3 (red) and either RPA, TEX11, MSH4 or RNF212 (green) following chemical inhibition of SUMO conjugation, ubiquitin conjugation or proteasomes. (**B, D, F** and **H**) Quantification of RPA, TEX11, MSH4 and RNF212 foci from the experiments represented in panels A, C, E and G, respectively. LZ, late zygonema; EP, early pachynema; MP, mid pachynema. Arrows indicates sex chromosomes. Error bars show mean ± s.d. (*) $P \leq 0.05$, (**) $P \leq 0.01$, (***) $P \leq 0.001$, two-tailed Mann-Whitney test. Scale bars = 10μm.

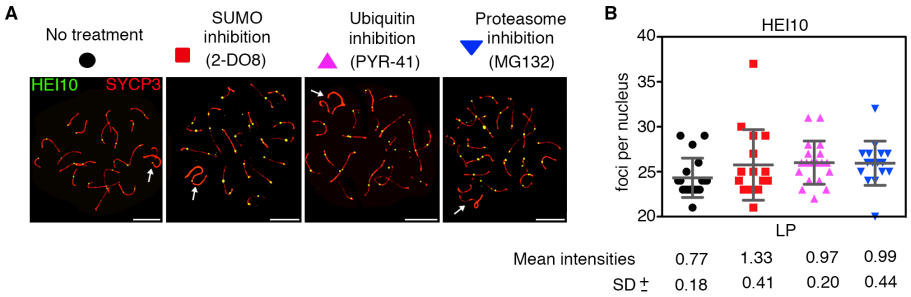

Fig. S9

HEI10 immunostaining following inhibition of the SMS and UPS.
(**A**) Representative late-pachynema spermatocyte nuclei immunostained for SYCP3 (red) and HEI10 (green) following chemical inhibition of SUMO conjugation, ubiquitin conjugation or proteasomes. (**B**) Quantification of HEI10 immunostaining foci. By two-tailed Mann-Whitney, HEI10 foci were significantly brighter following SUMO inhibition ($P \leq 0.001$), and maybe also following ubiquitin inhibition ($P \leq 0.05$), but not proteasome inhibition. Arrows indicates sex chromosomes. Error bars show mean ± s.d. Scale bars = 10μm.

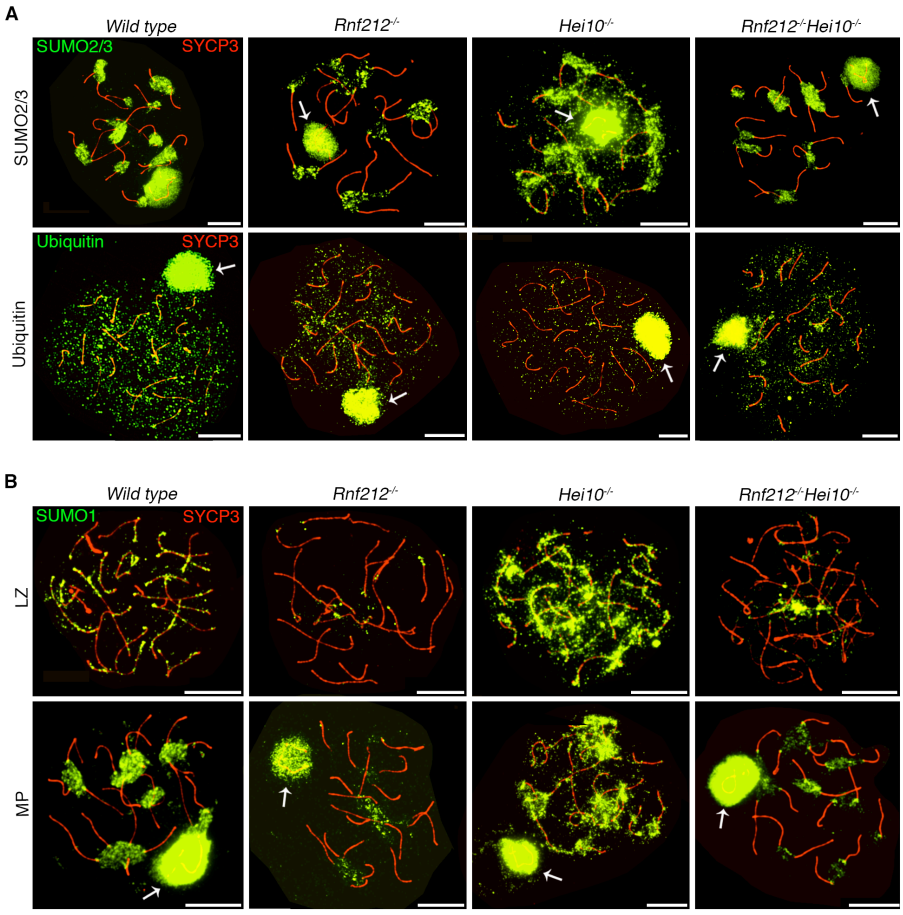

Fig. S10

SUMO and ubiquitin immunostaining in *Rnf212, Hei10* and *Rnf212 Hei10* mutants. (**A**) Representative mid/late-pachynema spermatocyte nuclei from the specified mouse strains immunotained for SUMO2/3 (upper panels) or ubiquitin (lower panels). While axial SUMO staining is diminished in zygotene *Rnf212*$^{-/-}$ mutant nuclei (Fig. 4A,B), later staining of the sex body and centromeric heterochromatin is still detected. In the *Hei10*$^{-/-}$ mutant, SUMO staining along autosomal axes persists throughout pachynema, concurrent with prominent sex body staining; this pattern is never observed in wild type nuclei. The *Rnf212*$^{-/-}$ *Hei10*$^{-/-}$ double mutant shows that this persistence is RNF212 dependent. Ubiquitin staining of autosomal axes is diminished in nuclei from all three mutants, but ubiquitin still accumulates on the chromatin of the sex body. (**B**) SUMO1 staining in representative nuclei from the specified mouse strains. Staining patterns and genetic dependencies are analogous to those observed for SUMO2/3. LZ, late zygonema; MP, mid pachynema. Arrows indicates sex chromosomes. Scale bars = 10μm.

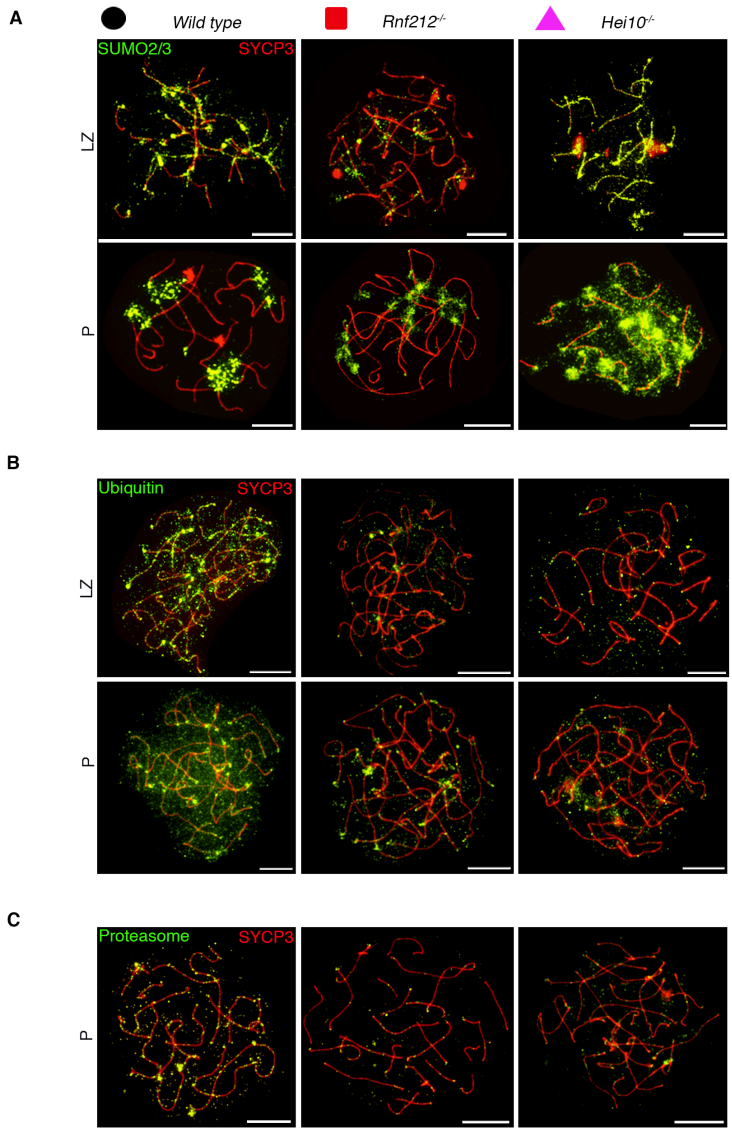

Fig. S11

In fetal oocytes, SUMO, ubiquitin and proteasomes decorate chromosome axes and are regulation by RNF212 and HEI10. (**A-C**) Representative oocyte nuclei from the indicated strains immunostained for the chromosome axis marker SYCP3 and either SUMO2/3 (**A**), ubiquitin (**B**) or the alpha subunit of the 20S proteasome core particle (**C**). The patterns and genetic dependencies mirror those seen for male meiosis, described in Figs. 1 and 4. Late zygonema (LZ), pachynema (P). Scale bars = 10μm.

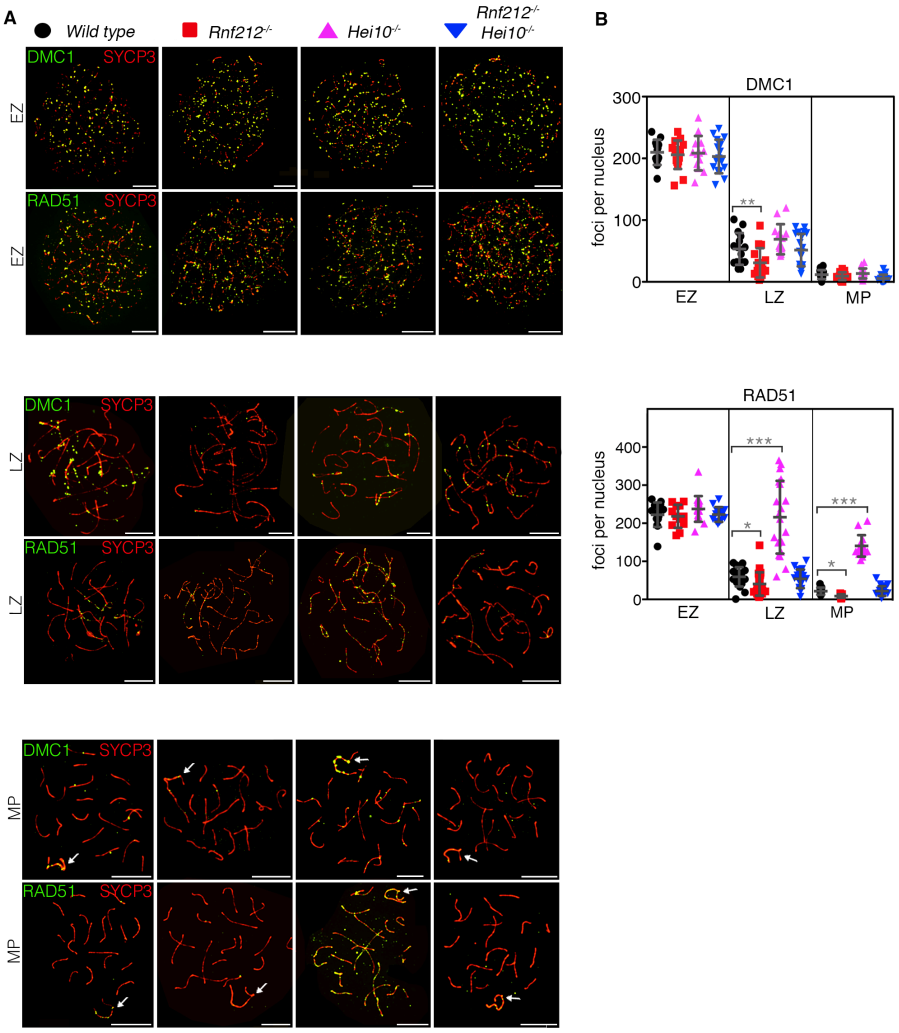

Fig. S12

RNF212 and HEI10 differentially regulate the turnover of DMC1 and RAD51. (**A**) Representative images of spermatocyte nuclei from the specified mouse strains immunostained for SYCP3 (red) and either DMC1 or RAD51 (green). Arrows indicates sex chromosomes. (**B**) Quantification of DMC1 and RAD51 foci from the experiments represented in (A). EZ, early zygonema; LZ, late zygonema; MP, mid pachynema. Error bars show mean ± s.d. (*) $P \leq 0.05$, (**) $P \leq 0.01$, (***) $P \leq 0.001$, two-tailed Mann-Whitney test. Scale bars = 10μm.

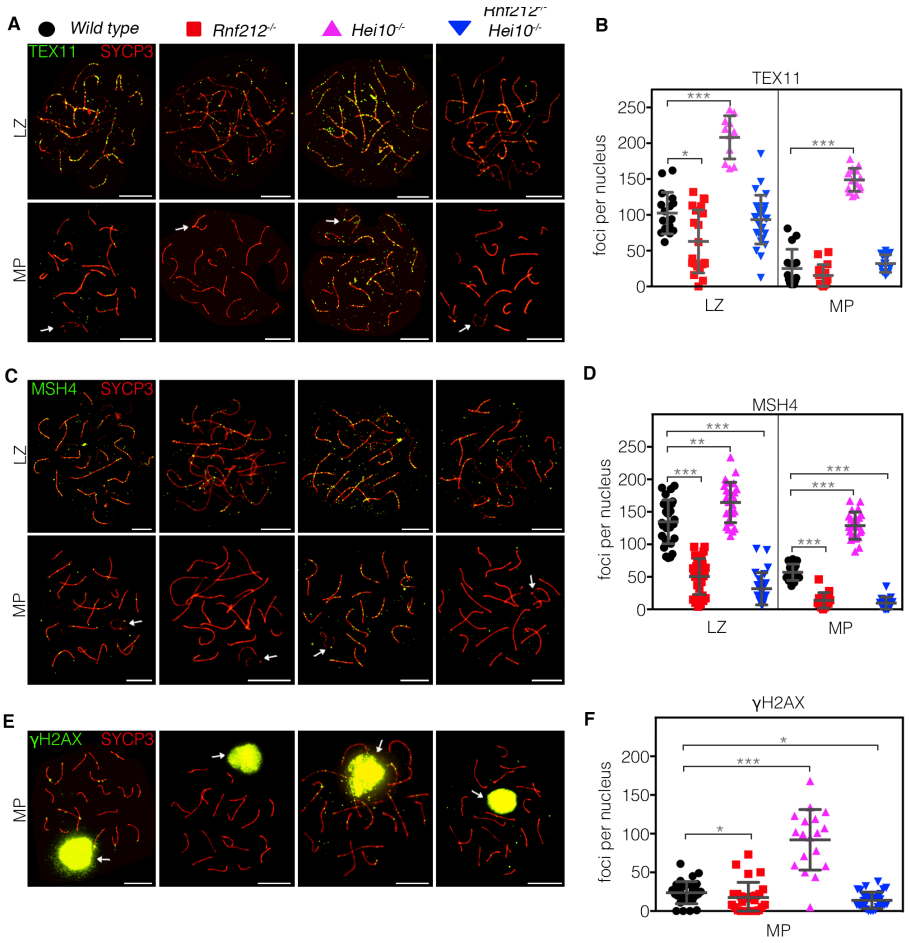

Fig. S13

Turnover of recombination proteins is regulated by the RNF212-HEI10 pathway. (**A, C,** and **E**) Representative images of spermatocyte nuclei from the specified mouse strains immunostained for SYCP3 (red) and either TEX11, MSH4 or γH2AX (green). (**B, D,** and **F**) Quantification of TEX11, MSH4 and gH2AX foci from the experiments represented in panels A, C and E, respectively. EZ, early zygonema; LZ, late zygonema; MP, mid pachynema. Arrows indicates sex chromosomes. Error bars show mean ± s.d. . (*) $P \leq 0.05$, (**) $P \leq 0.01$, (***) $P \leq 0.001$, two-tailed Mann-Whitney test. Scale bars = 10μm.

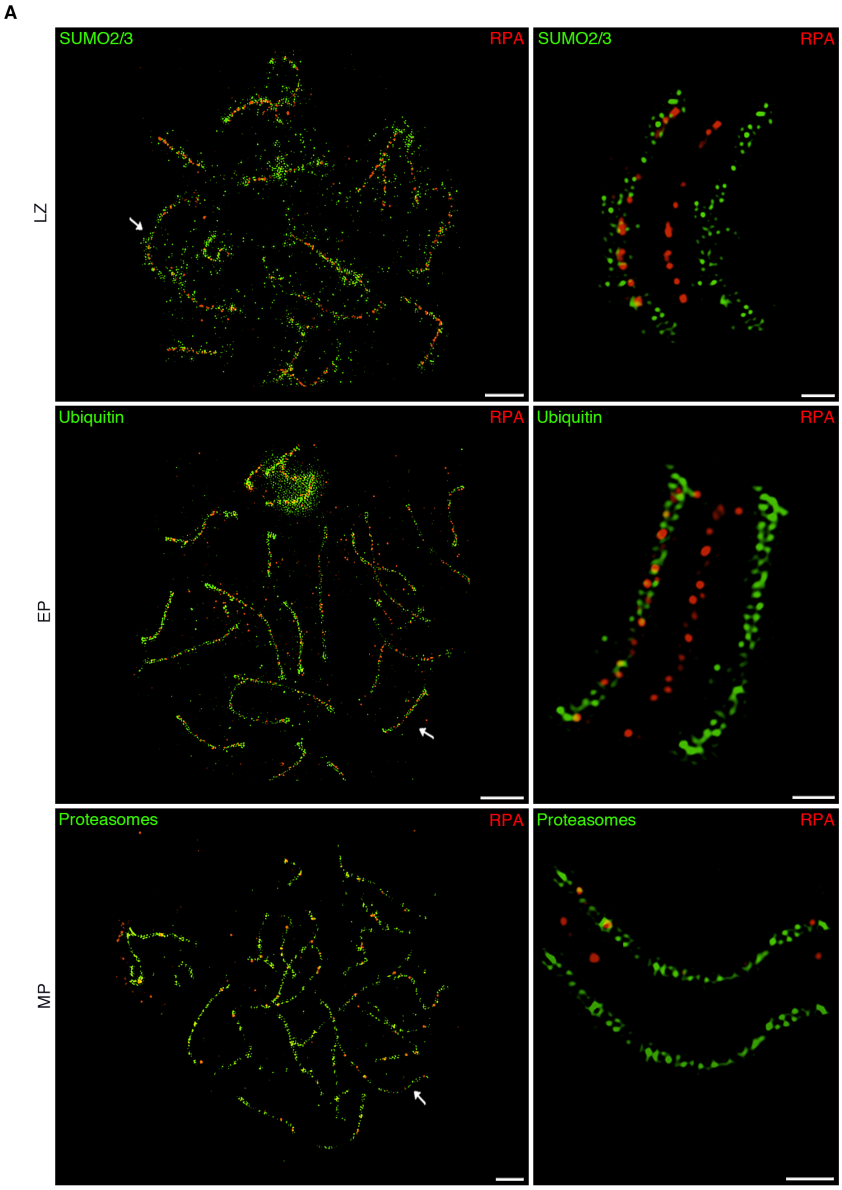

Fig. S14

Localization of recombination sites relative to SUMO, ubiquitin and proteasomes. SIM images of wild-type spermatocyte nuclei immunostained for RPA (red) and either SUMO2/3, ubiquitin, or 20S proteasome core particles (green). Arrows indicate the individual chromosomes magnified in the adjacent panels. Colocalization frequencies, defined as ≥50% overlap between signals, were 27.8 ± 1.5 % (n = X), 32.8 ± 3.0 % (n = X) and 37.8 ± 2.9 % (n = 5), respectively, for RPA colocalization with SUMO2/3, ubiquitin and proteasomes. LZ, late zygonema; EP, early pachynema; MP, mid pachynema; Scale bars = 5µm for full nuclei and 1µm for single chromosomes.

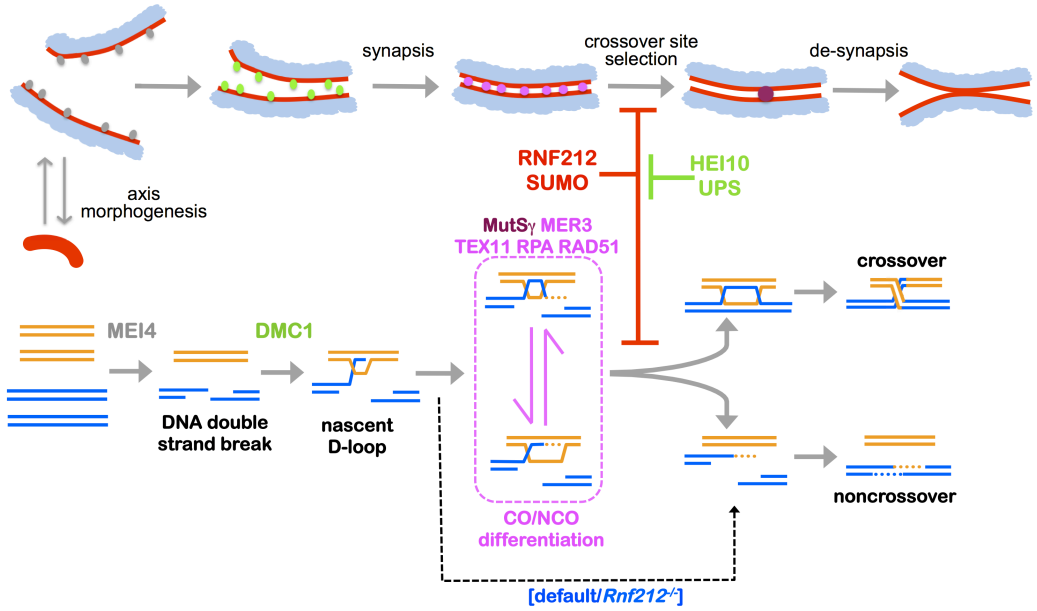

Fig. S15

Roles of the SMS and UPS during mammalian meiotic prophase and logic of the RNF212-HEI10 pathway. The top row represents the chromosomal events of meiotic prophase, highlighting the steps of meiotic prophase regulated by the SMS and UPS, and the dynamics of the recombination factors analyzed in this study. The bottom row shows the corresponding DNA events of meiotic recombination and the steps at which each factor is known or inferred to act. RNF212-dependent SUMOylation is proposed to be a prequisite for the selection of crossover sites, acting to stall recombination at a defined intermediate step, enabling regulated deselection of recombination sites via HEI10-mediated proteolysis. CO, crossover; NCO, noncrossover.

References and Notes

1. N. Hunter, Meiotic recombination: The essence of heredity. *Cold Spring Harb. Perspect. Biol.* **7**, a016618 (2015). Medline

2. S. Jentsch, I. Psakhye, Control of nuclear activities by substrate-selective and protein-group SUMOylation. *Annu. Rev. Genet.* **47**, 167–186 (2013). doi:10.1146/annurev-genet-111212-133453 Medline

3. K. Eifler, A. C. Vertegaal, SUMOylation-mediated regulation of cell cycle progression and cancer. *Trends Biochem. Sci.* **40**, 779–793 (2015). doi:10.1016/j.tibs.2015.09.006 Medline

4. P. W. Brown, K. Hwang, P. N. Schlegel, P. L. Morris, Small ubiquitin-related modifier (SUMO)-1, SUMO-2/3 and SUMOylation are involved with centromeric heterochromatin of chromosomes 9 and 1 and proteins of the synaptonemal complex during meiosis in men. *Hum. Reprod.* **23**, 2850–2857 (2008). doi:10.1093/humrep/den300 Medline

5. F. Z. Watts, E. Hoffmann, SUMO meets meiosis: An encounter at the synaptonemal complex. *BioEssays* **33**, 529–537 (2011). doi:10.1002/bies.201100002 Medline

6. R. Bose, G. Manku, M. Culty, S. S. Wing, Ubiquitin-proteasome system in spermatogenesis. *Adv. Exp. Med. Biol.* **759**, 181–213 (2014). doi:10.1007/978-1-4939-0817-2_9 Medline

7. M. T. Jahns, D. Vezon, A. Chambon, L. Pereira, M. Falque, O. C. Martin, L. Chelysheva, M. Grelon, Crossover localisation is regulated by the neddylation posttranslational regulatory pathway. *PLOS Biol.* **12**, e1001930 (2014). doi:10.1371/journal.pbio.1001930 Medline

8. L. Zhang, S. Wang, S. Yin, S. Hong, K. P. Kim, N. Kleckner, Topoisomerase II mediates meiotic crossover interference. *Nature* **511**, 551–556 (2014). doi:10.1038/nature13442 Medline

9. A. Rodriguez, S. A. Pangas, Regulation of germ cell function by SUMOylation. *Cell Tissue Res.* **363**, 47–55 (2016). Medline

10. S. La Salle, F. Sun, X. D. Zhang, M. J. Matunis, M. A. Handel, Developmental control of sumoylation pathway proteins in mouse male germ cells. *Dev. Biol.* **321**, 227–237 (2008). doi:10.1016/j.ydbio.2008.06.020 Medline

11. W. M. Baarends, J. W. Hoogerbrugge, H. P. Roest, M. Ooms, J. Vreeburg, J. H. J. Hoeijmakers, J. A. Grootegoed, Histone ubiquitination and chromatin remodeling in mouse spermatogenesis. *Dev. Biol.* **207**, 322–333 (1999). doi:10.1006/dbio.1998.9155 Medline

12. J. S. Ahuja, R. Sandhu, R. Mainpal, C. Lawson, H. Henley, P. A. Hunt, J. L. Yanowitz, G. V. Börner, Control of meiotic pairing and recombination by chromosomally tethered 26*S* proteasome. *Science* **355**, 408–411 (2017). DOI:10.1126/science.aaf47778

13. K. Newton, M. L. Matsumoto, I. E. Wertz, D. S. Kirkpatrick, J. R. Lill, J. Tan, D. Dugger, N. Gordon, S. S. Sidhu, F. A. Fellouse, L. Komuves, D. M. French, R. E. Ferrando, C. Lam, D. Compaan, C. Yu, I. Bosanac, S. G. Hymowitz, R. F. Kelley, V. M. Dixit, Ubiquitin

chain editing revealed by polyubiquitin linkage-specific antibodies. *Cell* **134**, 668–678 (2008). doi:10.1016/j.cell.2008.07.039 Medline

14. S. La Salle, F. Sun, M. A. Handel, Isolation and short-term culture of mouse spermatocytes for analysis of meiosis. *Methods Mol. Biol.* **558**, 279–297 (2009). doi:10.1007/978-1-60761-103-5_17 Medline

15. Y. S. Kim, K. Nagy, S. Keyser, J. S. Schneekloth Jr., An electrophoretic mobility shift assay identifies a mechanistically unique inhibitor of protein sumoylation. *Chem. Biol.* **20**, 604–613 (2013). doi:10.1016/j.chembiol.2013.04.001 Medline

16. Y. Yang, J. Kitagaki, R.-M. Dai, Y. C. Tsai, K. L. Lorick, R. L. Ludwig, S. A. Pierre, J. P. Jensen, I. V. Davydov, P. Oberoi, C.-C. H. Li, J. H. Kenten, J. A. Beutler, K. H. Vousden, A. M. Weissman, Inhibitors of ubiquitin-activating enzyme (E1), a new class of potential cancer therapeutics. *Cancer Res.* **67**, 9472–9481 (2007). doi:10.1158/0008-5472.CAN-07-0568 Medline

17. J. L. Syrjänen, L. Pellegrini, O. R. Davies, A molecular model for the role of SYCP3 in meiotic chromosome organisation. *eLife* **3**, e02963 (2014). doi:10.7554/eLife.02963 Medline

18. H. Brockway, N. Balukoff, M. Dean, B. Alleva, S. Smolikove, The CSN/COP9 signalosome regulates synaptonemal complex assembly during meiotic prophase I of *Caenorhabditis elegans*. *PLOS Genet.* **10**, e1004757 (2014). doi:10.1371/journal.pgen.1004757 Medline

19. R. Kumar, H. M. Bourbon, B. de Massy, Functional conservation of Mei4 for meiotic DNA double-strand break formation from yeasts to mice. *Genes Dev.* **24**, 1266–1280 (2010). doi:10.1101/gad.571710 Medline

20. M. S. Brown, D. K. Bishop, DNA strand exchange and RecA homologs in meiosis. *Cold Spring Harb. Perspect. Biol.* **7**, a016659 (2014). doi:10.1101/cshperspect.a016659 Medline

21. H. Qiao, H. B. D. Prasada Rao, Y. Yang, J. H. Fong, J. M. Cloutier, D. C. Deacon, K. E. Nagel, R. K. Swartz, E. Strong, J. K. Holloway, P. E. Cohen, J. Schimenti, J. Ward, N. Hunter, Antagonistic roles of ubiquitin ligase HEI10 and SUMO ligase RNF212 regulate meiotic recombination. *Nat. Genet.* **46**, 194–199 (2014). doi:10.1038/ng.2858 Medline

22. A. Reynolds, H. Qiao, Y. Yang, J. K. Chen, N. Jackson, K. Biswas, J. K. Holloway, F. Baudat, B. de Massy, J. Wang, C. Höög, P. E. Cohen, N. Hunter, RNF212 is a dosage-sensitive regulator of crossing-over during mammalian meiosis. *Nat. Genet.* **45**, 269–278 (2013). doi:10.1038/ng.2541 Medline

23. A. De Muyt, L. Zhang, T. Piolot, N. Kleckner, E. Espagne, D. Zickler, E3 ligase Hei10: A multifaceted structure-based signaling molecule with roles within and beyond meiosis. *Genes Dev.* **28**, 1111–1123 (2014). doi:10.1101/gad.240408.114 Medline

24. V. Cloud, Y. L. Chan, J. Grubb, B. Budke, D. K. Bishop, Rad51 is an accessory factor for Dmc1-mediated joint molecule formation during meiosis. *Science* **337**, 1222–1225 (2012). doi:10.1126/science.1219379 Medline

25. O. Da Ines, F. Degroote, C. Goubely, S. Amiard, M. E. Gallego, C. I. White, Meiotic recombination in *Arabidopsis* is catalysed by DMC1, with RAD51 playing a supporting role. *PLOS Genet.* **9**, e1003787 (2013). doi:10.1371/journal.pgen.1003787 Medline

26. D. Zickler, N. Kleckner, Recombination, pairing, and synapsis of homologs during meiosis. *Cold Spring Harb. Perspect. Biol.* **7**, a016626 (2015). doi:10.1101/cshperspect.a016626 Medline

27. A. M. Sriramachandran, R. J. Dohmen, SUMO-targeted ubiquitin ligases. *Biochim. Biophys. Acta* **1843**, 75–85 (2014). doi:10.1016/j.bbamcr.2013.08.022 Medline

28. C. H. Freudenreich, X. A. Su, Relocalization of DNA lesions to the nuclear pore complex. *FEMS Yeast Res.* **16**, fow095 (2016). doi:10.1093/femsyr/fow095 Medline

29. J. O. Ward, L. G. Reinholdt, W. W. Motley, L. M. Niswander, D. C. Deacon, L. B. Griffin, K. K. Langlais, V. L. Backus, K. J. Schimenti, M. J. O'Brien, J. J. Eppig, J. C. Schimenti, Mutation in mouse hei10, an e3 ubiquitin ligase, disrupts meiotic crossing over. *PLOS Genet.* **3**, e139 (2007). doi:10.1371/journal.pgen.0030139 Medline

30. J. K. Holloway, J. Booth, W. Edelmann, C. H. McGowan, P. E. Cohen, MUS81 generates a subset of MLH1-MLH3-independent crossovers in mammalian meiosis. *PLOS Genet.* **4**, e1000186 (2008). doi:10.1371/journal.pgen.1000186 Medline

31. X. Sun, P. E. Cohen, Studying recombination in mouse oocytes. *Methods Mol. Biol.* **957**, 1–18 (2013). doi:10.1007/978-1-62703-191-2_1 Medline

32. H. Qiao, L. D. Lohmiller, L. K. Anderson, Cohesin proteins load sequentially during prophase I in tomato primary microsporocytes. *Chromosome Res.* **19**, 193–207 (2011). doi:10.1007/s10577-010-9184-1 Medline

33. M. J. Matunis, E. Coutavas, G. Blobel, A novel ubiquitin-like modification modulates the partitioning of the Ran-GTPase-activating protein RanGAP1 between the cytosol and the nuclear pore complex. *J. Cell Biol.* **135**, 1457–1470 (1996). doi:10.1083/jcb.135.6.1457 Medline

34. X. D. Zhang, J. Goeres, H. Zhang, T. J. Yen, A. C. G. Porter, M. J. Matunis, SUMO-2/3 modification and binding regulate the association of CENP-E with kinetochores and progression through mitosis. *Mol. Cell* **29**, 729–741 (2008). doi:10.1016/j.molcel.2008.01.013 Medline

35. F. Yang, K. Gell, G. W. van der Heijden, S. Eckardt, N. A. Leu, D. C. Page, R. Benavente, C. Her, C. Höög, K. J. McLaughlin, P. J. Wang, Meiotic failure in male mice lacking an X-linked factor. *Genes Dev.* **22**, 682–691 (2008). doi:10.1101/gad.1613608 Medline

36. M. Eijpe, H. Offenberg, R. Jessberger, E. Revenkova, C. Heyting, Meiotic cohesin REC8 marks the axial elements of rat synaptonemal complexes before cohesins SMC1beta and SMC3. *J. Cell Biol.* **160**, 657–670 (2003). doi:10.1083/jcb.200212080 Medline

37. T. Ashley, A. P. Gaeth, L. B. Creemers, A. M. Hack, D. G. de Rooij, Correlation of meiotic events in testis sections and microspreads of mouse spermatocytes relative to the mid-pachytene checkpoint. *Chromosoma* **113**, 126–136 (2004). doi:10.1007/s00412-004-0293-5 Medline

38. T. Wiltshire, C. Park, K. A. Caldwell, M. A. Handel, Induced premature G_2/M-phase transition in pachytene spermatocytes includes events unique to meiosis. *Dev. Biol.* **169**, 557–567 (1995). doi:10.1006/dbio.1995.1169 Medline